

We are IntechOpen, the world's leading publisher of Open Access books Built by scientists, for scientists

5,000

Open access books available

124,000

International authors and editors

140M

Downloads

Our authors are among the

154

Countries delivered to

TOP 1%

most cited scientists

12.2%

Contributors from top 500 universities



WEB OF SCIENCE™

Selection of our books indexed in the Book Citation Index
in Web of Science™ Core Collection (BKCI)

Interested in publishing with us?
Contact book.department@intechopen.com

Numbers displayed above are based on latest data collected.
For more information visit www.intechopen.com



Photonic Metamaterials: Controlling Nanoscale Radiative Thermal Transport

Alok Ghanekar, Yanpei Tian and Yi Zheng

Additional information is available at the end of the chapter

<http://dx.doi.org/10.5772/intechopen.72805>

Abstract

We discuss concepts of radiative thermal diodes demonstrating dynamic control and modulation of radiative heat transfer. These concepts are analogous to electronic diodes and display high degree of asymmetry in radiative heat transfer. Change in optical properties of vanadium dioxide (VO₂) upon phase transition are exploited to influence thermal radiation. The first concept is based on a simple multi-layer structure containing a layer of VO₂ to attain dynamic optical response in the far-field regime. The active terminal of the diode changes from highly reflecting to highly absorbing upon phase transition of VO₂. In the second concept, a near-field thermal diode is considered that utilizes period gratings of VO₂. Radiative heat transfer across the near-field gap is modulated by altering tunneling of surface waves when phase change in VO₂ occurs. For minimal temperature difference of 20 K, rectification ratios have been reported and they are maximum in existing literature for comparable operating temperatures and configurations.

Keywords: metamaterials, near-field, far-field, thermal diode, radiative thermal transport

1. Introduction

Thermal diode [1], thermal transistors [2], thermal memory element [3] and similar thermal analogues of electronic devices have been topic of theoretical as well as experimental works. While earlier research has been on conduction (phonon) based devices [4–8], more recent studies have been focusing on radiation (photon) based thermal rectifiers [9–12]. Thermal rectification has numerous applications in thermal management, thermal logic gates [13–15] and information processing [16].

Analogous to electrical diode, thermal diode is a rectification device wherein magnitude of heat flux strongly depends on the sign of applied temperature bias. To quantify rectification, one can employ the widely used definition of rectification ratio, i.e., $R = (Q_f - Q_r)/Q_r$ where

Q_f and Q_r refer to forward and reverse heat flux, respectively [17]. Alternatively, rectification coefficient can be defined as $\eta = (Q_f - Q_r)/\max(Q_r, Q_f)$. There are numerous studies pertaining to near-field and far-field thermal radiation based rectification devices that exploit temperature dependent properties of a phase change materials such as vanadium dioxide (VO_2) and $\text{La}_{0.7}\text{Ca}_{0.15}\text{Sr}_{0.15}\text{MnO}_3$ (LCSMO) [11, 18, 19]. A number of studies deal with far-field thermal radiation [20, 21] while several others focus on modulation of radiative heat transfer in the near-field regime [18, 19, 22–26]. Ben-Abdallah and Biehs introduced a VO_2 based simple far-field radiative thermal diode, while Prod'homme et al. [27] proposed a far-field thermal transistor that uses a VO_2 base between a blackbody collector and a blackbody emitter. Zhu et al. [28] showed that temperature dependent optical properties of SiC can be used to attain negative differential conductance. Van Zwol et al. [22] proposed that one can take advantage of the phase transition from crystalline to amorphous state in AIST (an alloy of Ag, In, Sb, and Te) driven by a current pulse to obtain a large contrast in heat flux. In far-field limit, rectification is due to the change in emissive properties of a phase change material. In near-field limit, the difference in the coupling strength of polaritons or tunneling of surface waves between structures leads to thermal rectification. In general, it is observed that a higher rectification can be achieved in the near-field regime than in the far-field. However, it is challenging to develop such devices operating on the principle of near-field radiative transfer.

Spectral control has been studied to affect radiative heat transfer in both the far-field as well as near-field. Customization of absorption/emission spectra is often achieved by the use of multilayer thin film structures [29], nanoparticles [30, 31], dielectric mixtures [32, 33], photonic crystals [34, 35], 1-D/2-D gratings [36] and metamaterials [37, 38]. Absorbers that utilize Fabry-Perot cavities [39, 40], Salisbury screens [41] and Jaumann absorbers [42] and ultra-thin lossy thin films bounded by transparent substrate and superstrate [43–45] have been investigated for decades. Quite notably, Nefzaoui et al. [46] proposed using multilayer structures consisting of thin films (e.g., Si, HDSi and gold) to obtain thermal rectification. Kats et al. [47] have theoretically and experimentally demonstrated that a thin-film of VO_2 on sapphire shows strong modulation of absorbance upon phase transition, particularly, at wavelength of $11.6\text{ }\mu\text{m}$. Taylor et al. [48] recently proposed an emitter consisting a dielectric spacer between VO_2 film and a reflecting substrate to achieve dynamic radiative cooling upon phase transition of VO_2 . Fabry-Perot resonance was achieved at $10\text{ }\mu\text{m}$ wavelength. We will see that, by tuning the resonance at right wavelength, maximum rectification can be achieved in the proposed design.

VO_2 has often been used in thermal rectification devices, because its phase-change from an insulator to a metal can be switched reversibly within a short time ($\sim 100\text{ fs}$) [49]. The common devices use either a bulk VO_2 solid or its thin-film form. Here, we will see two cases of radiative thermal diodes with record rectification ratios achieved when compared to similar operating conditions and configurations.

2. Far-field thermal diode

A typical far-field thermal diode has two planar components separated by a distance much larger than thermal wavelength. The active component is made of a phase-change solid,

whereas the passive component stays inert. **Figure 1** illustrates the vertical structure of the proposed thermal diode. The active component contains a tri-layer structure consisting of VO₂, potassium bromide (KBr) and gold thin films on a substrate. Thicknesses of VO₂ and KBr layers can be tuned to maximize rectification. The thickness of gold layer is fixed at 1 μm to block radiation from the substrate. For a given temperature bias, maximum (far-field) radiative heat transfer would be possible when both sides are blackbodies, while minimum heat transfer would take place when at least one side is a highly reflective mirror. Ideally, the active component should exhibit a transition from blackbody to reflective surface upon the reversal of a temperature bias which induces the phase change. This is exactly what the design attempts to achieve. Therefore, the passive component is chosen to be a blackbody. Any material other than a blackbody would not yield the maximum rectification. Structures 1 and 2 are at temperature $T_1 = T_c + \Delta T$ and $T_2 = T_c - \Delta T$, respectively. The mean temperature is chosen to be the phase transition temperature of VO₂ ($T = 341$ K). When $T_1 > T_2$ (referred to as forward bias), VO₂ layer is in its metallic phase; and when $T_1 < T_2$ (reverse bias), VO₂ layer becomes insulating with its optical axis aligned along the vertical direction, i.e., z-axis.

Phase transition of VO₂ is not abrupt [49, 50] and a complete insulator-metal transition does not occur until 350 K [26]. Rectification ratio depends on temperature bias as the temperature

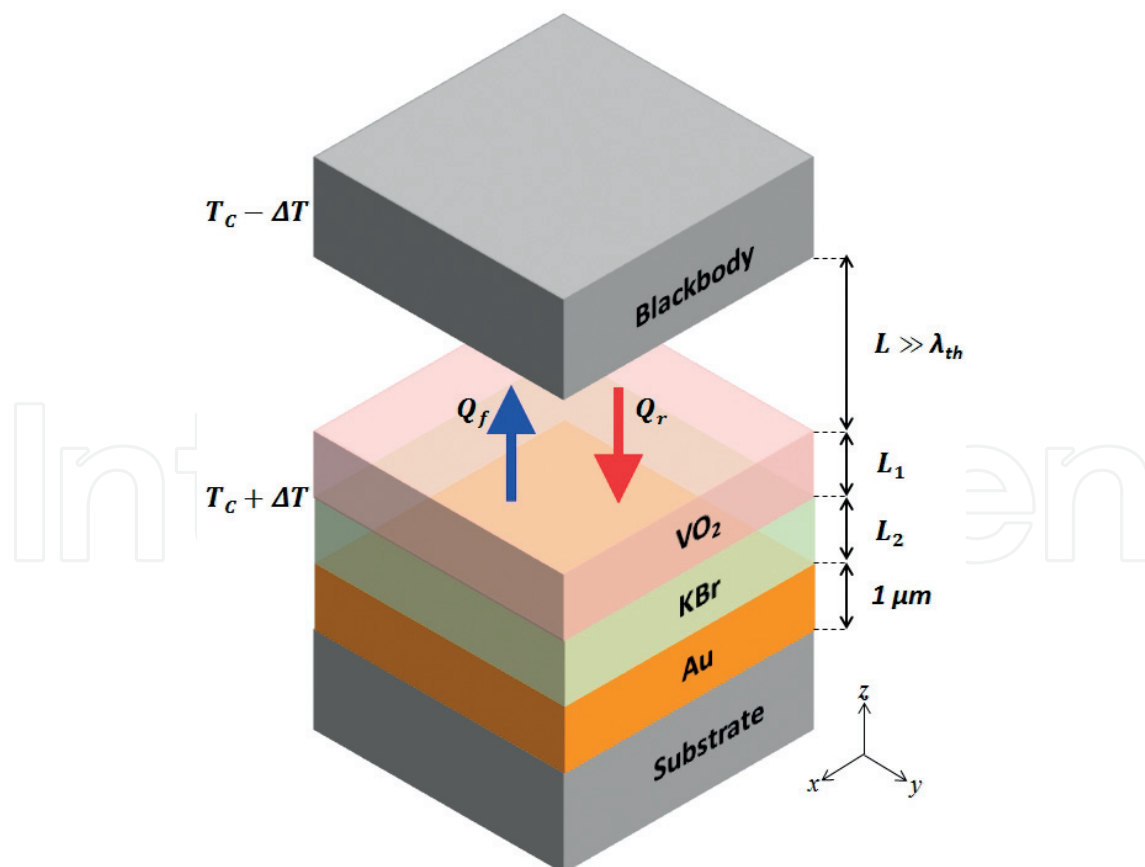


Figure 1. Schematic of a far-field thermal diode with a high rectification ratio. The active component has a tri-layer structure consisting of VO₂, KBr and gold thin films on a substrate with thicknesses L_1 , L_2 and $1\ \mu\text{m}$, respectively. The passive component is a blackbody. $T_c = 341$ K is the phase transition temperature of VO₂.

dependence of radiative heat transfer is essentially nonlinear. Here, rectification values are calculated at a minimal temperature bias of 20 K i.e., $\Delta T = \pm 10$ K. Although transition of VO_2 exhibits a thermal hysteresis of about 8 K as presented in Refs. [49, 51], the phase transition is reversible. As we are concerned with heat flux values at 10 K above and below the critical temperature of VO_2 , hysteresis behavior is ignored for the sake of simplicity. A multilayer structure can be designed to attain high absorbance or reflectance based on its dimensions and material properties. Multilayers with constituent thicknesses much smaller than the incident wavelength of light have been studied before [52]. Here, we see that in a VO_2 based multilayer structure, the dramatic change in the optical property of VO_2 upon phase-change facilitates an extensive variation in the surface reflectivity.

Concept shown in **Figure 1** has variable dimensions of VO_2 (L_1) and KBr (L_2) layer. These dimensions can be optimized by running Genetic Algorithm to maximize rectification ratio. When lower and upper bounds on L_1 and L_2 are kept at 25 nm and 2 μm , respectively, optimal dimensions can be found to be $L_1 = 25$ and $L_2 = 880$ nm, both are practical values. Further discussion will be focused on the design with these dimensions. **Figure 2** shows spectral heat flux ($dq/d\lambda$) of the proposed thermal diode in forward and reverse direction with temperature bias 20 K ($\Delta T = 10$ K). Forward heat flux is significantly higher than reverse flux as is clear from **Figure 2**. A comparison is shown for heat flux across blackbodies at temperatures 331 and 351 K, respectively. Inset in **Figure 2** displays angle-averaged emissivity of the active component in both scenarios. When VO_2 is metallic, the structure on the active component has high emissivity near the thermal wavelength ($\lambda_{\text{th}} = 1.27hc/k_B T = 8.5 \mu\text{m}$ for 341 K). As a significant portion of blackbody radiation falls within this range, this gives rise to a high heat flux in forward bias. However, when VO_2 is insulating, the structure has very low emissivity in the broad spectrum. The tri-layer structure behaves like a highly reflecting mirror resulting in very low heat flux. Consequently, high contrast in heat flow is achieved leading to a high rectification ratio of 11.3 ($\eta = 0.918$). In order to highlight the diode-like characteristics, heat flux across the device has been plotted against temperature difference in **Figure 3**. For comparison, simple case of bulk VO_2 is also shown, it has a rectification coefficient of $\eta = 0.49$.

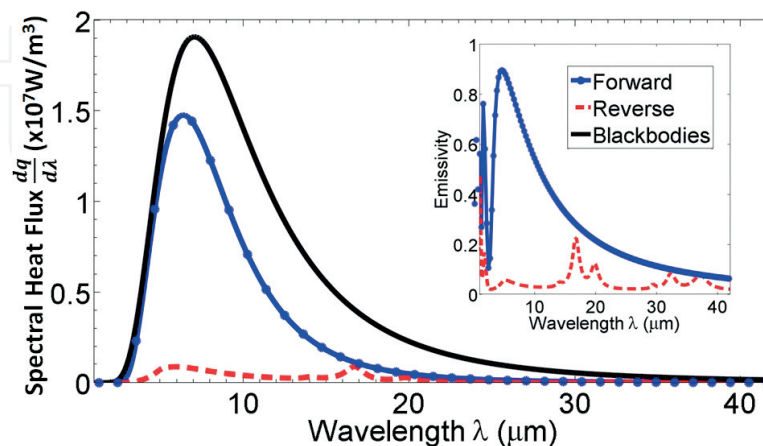


Figure 2. Spectral heat flux across the optimized thermal diode in forward and reverse bias scenarios. Spectral heat flux between blackbodies at temperatures 331 and 351 K is shown for reference. Inset shows hemispherical emissivity of the active component of the diode for the forward and reverse bias.

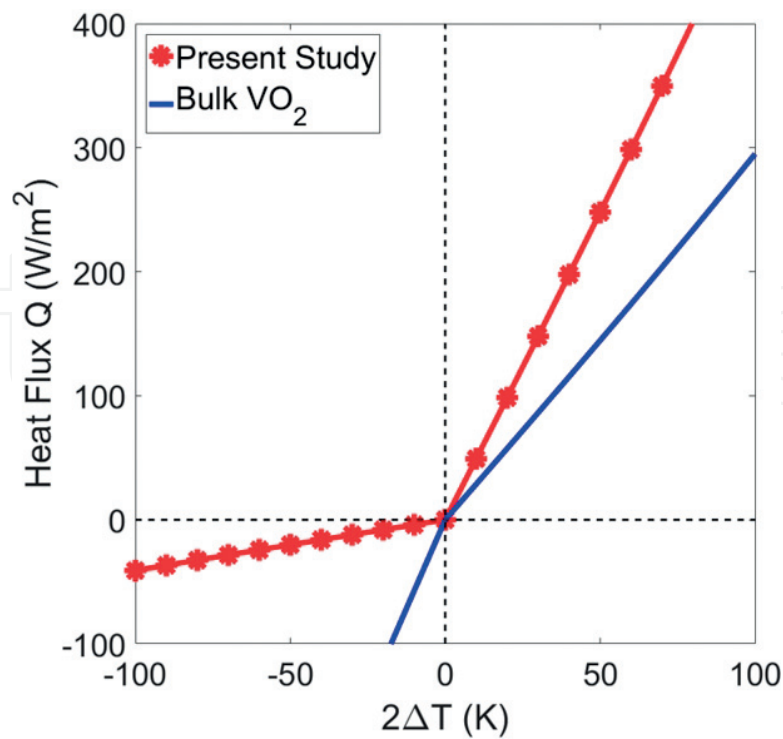


Figure 3. Heat flux plotted against temperature difference for thermal diode with bulk VO₂ and present structure.

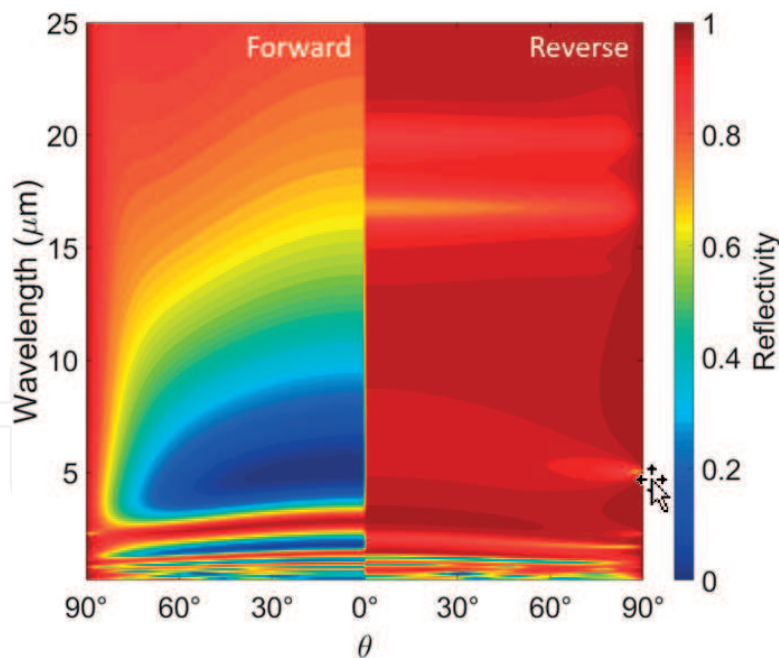


Figure 4. Angle dependent reflectivity of the active component of thermal diode plotted against wavelength and angle of incidence under forward and reverse bias.

Angle dependent spectral reflectivity of the active component of the thermal diode is plotted in **Figure 4** for the forward and reverse bias cases. When VO₂ is metallic, the tri-layer structure acts like a wide-angle antireflection coating for wavelengths between 4 and 10 μm. The dark

spot in **Figure 4** corresponds to Fabry-Perot type of resonance that occurs around $\lambda = 4n_{\text{KBr}}(\lambda)L_2 = 5.3 \text{ } \mu\text{m}$ [47]. High absorption/emission in this wavelength region favors radiative heat transfer as thermal wavelength falls within this range. In reverse bias, the structure is highly reflective in a broad range of wavelengths giving rise to a very low absorption. Note that for thermal wavelength of $8.5 \text{ } \mu\text{m}$, Fabry-Perot resonance occurs (for metallic VO_2) when thickness of KBr layer is $L_2 = \lambda_{\text{th}}/4n_{\text{KBr}}(\lambda_{\text{th}}) = 1.4 \text{ } \mu\text{m}$. This configuration, however, would not necessarily achieve maximum rectification as the structure may not be purely reflecting when VO_2 is its insulating phase.

Contrasting reflective properties of the structure are due to constructive and destructive interferences of electromagnetic waves generated by partial reflections at interfaces. As an electromagnetic wave travels through the media, it is partially reflected at each interface leading to multiple reflections from each layer. This causes interference of electromagnetic waves due to each partial reflection. Effective reflection coefficient of the structure is the phasor sum of these reflection coefficients due to (an infinite number of) individual reflections. When VO_2 is metallic, phasor sum of partial reflections results in destructive interference in the wavelength range of $4 \text{ } \mu\text{m}$ to $10 \text{ } \mu\text{m}$. As a result, the structure is highly absorptive in the range. When VO_2 is insulating, individual reflections add up to a large value making the structure highly reflective for a broad range of the spectrum.

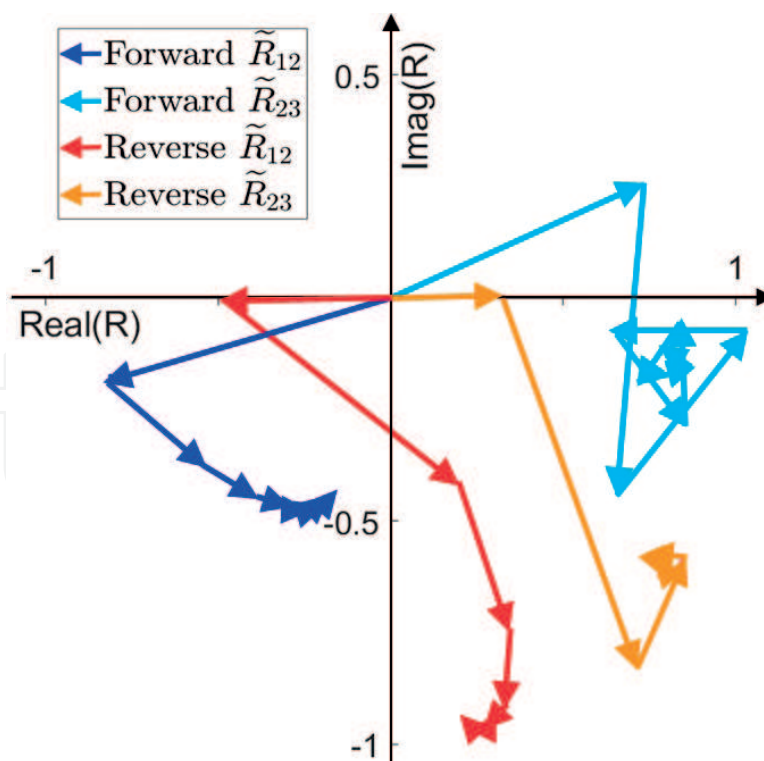


Figure 5. Effective reflection coefficient at air- VO_2 interface ($\tilde{R}_{1,2}$) and VO_2 -KBr interface ($\tilde{R}_{2,3}$) as phasor sum of reflection coefficients due to each reflection for TE polarized incident plane wave of wavelength $\lambda_{\text{th}} = 8.5 \text{ } \mu\text{m}$ and angle of incidence 10° .

Figure 5 shows phasor diagram of partial reflections at air-VO₂ interface and VO₂-KBr interface for TE polarized incident ray of wavelength $\lambda_{th} = 8.5 \mu\text{m}$ and angle of incidence 10° . $\tilde{R}_{1,2}$ is the effective reflection coefficient at air-VO₂ interface and $\tilde{R}_{2,3}$ is the effective reflection coefficient at VO₂-KBr interface due to multiple reflections within KBr layer. They can be expressed as geometric series whose terms are relative amplitudes of partial waves due to first, second and third reflection and so on. For both metallic as well as insulating VO₂, the magnitude of $\tilde{R}_{2,3}$, $|\tilde{R}_{2,3}|$, is large. However, when VO₂ is in metallic phase, each partial reflection results in a phase-shift such that partial waves add up destructively leading to a small value of $|\tilde{R}_{1,2}|$ and low reflectivity, especially in the wavelength range centered around thermal wavelength. On the other hand, in reverse bias (insulating VO₂) phasors add constructively, giving rise to highly reflective surface properties for a broad range of wavelengths. A similar phenomenon can be observed for TM polarization as well. As KBr is transparent and has a negligible extinction coefficient for most of infrared region, much of the absorption takes place within the VO₂ layer. Transparent layer of KBr mainly influences the reflective properties by altering the phase of the light propagating through the media. Potentially, any other material transparent to infrared light such as magnesium fluoride or intrinsic silicon can be used in this concept. However, optimal dimensions of such a device might be different.

3. Near-field thermal diode

In a near-field radiative thermal diode the two terminals are separated by a distance less than thermal wavelength [18]. The active side has a phase change material and its counterpart has fixed material properties. **Figure 6** introduces two concepts of thermal diode that consist of two structures at a distance of $L = 100 \text{ nm}$. In both concepts, structure 1 (active side) contains top layer of phase change material VO₂ at temperature $T_1 = 341 \text{ K} + \Delta T$. On the passive side, structure 2 has its temperature $T_2 = 341 \text{ K} - \Delta T$. Mean temperature is chosen to be the phase transition temperature of VO₂ at 341 K. When $T_1 > T_2$ (forward bias), VO₂ layer is in metallic phase; when $T_1 < T_2$ (reverse bias), VO₂ layer is in insulator phase with its optical axis aligned along the distance between them. Proposed configurations will be discussed in more details along with results.

In order to explain the results of the calculations for the proposed designs shown in **Figure 6**, rectification ratio against gap for four different configurations has been plotted in **Figure 7** for the temperature difference of 20 K ($\Delta T = \pm 10 \text{ K}$). Before discussing the main design (**Figure 6(a)**) we consider the simplistic case which consists of bulk VO₂ on active side and bulk BN on passive side (case I). As insulator VO₂ and metallic VO₂ have different optical properties, one expects to observe some degree of asymmetry in heat flow. Such a configuration exhibits weak rectification which gradually increases at smaller gaps when surface waves become dominant. Next we consider using thin films. In case II, the active side has $1 \mu\text{m}$ layer of VO₂ over $1 \mu\text{m}$ thick gold and the passive side has $1 \mu\text{m}$ layer of BN on the top of $1 \mu\text{m}$ gold. $1 \mu\text{m}$ thick layer of gold is sufficient to block radiation from the substrate and to support the top layer as free standing thin layer is not practical [53]. This design shows an increased near-field rectification,

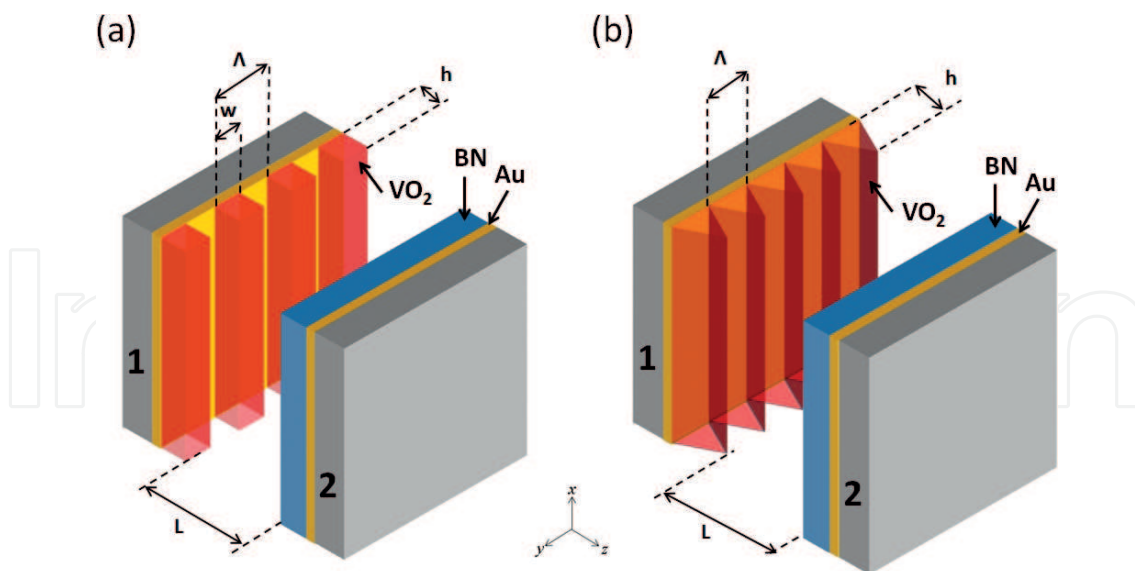


Figure 6. Schematics of near-field thermal diodes. (a) Active side has top layer of 1-D rectangular grating made of VO_2 of height h , width w , period Λ and filling ratio ϕ on a gold layer deposited on a substrate. (b) Rectangular grating is replaced by a triangular one of height h and period Λ . Passive counterpart of both designs consists of a BN layer on gold on the top of a substrate.

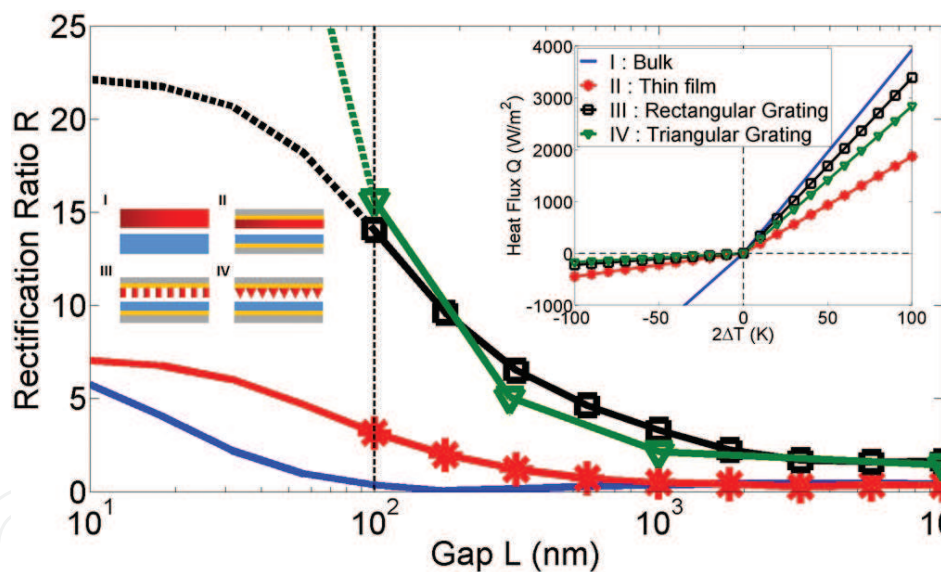


Figure 7. Gap-dependent rectification ratio for different thermal diode configurations. Passive structures are (I): Bulk BN, and (II), (III), (IV): $1\text{ }\mu\text{m}$ layer of BN over $1\text{ }\mu\text{m}$ layer of gold on a substrate. Active structures are (I): Bulk VO_2 , (II): $1\text{ }\mu\text{m}$ layer of VO_2 on the top of $1\text{ }\mu\text{m}$ layer of gold on a substrate, (III): Rectangular 1-D grating of VO_2 with thickness $h = 0.5\text{ }\mu\text{m}$, period $\Lambda = 50\text{ nm}$ and filling ratio $\phi = 0.3$, (IV): Triangular grating of VO_2 with height $h = 0.5\text{ }\mu\text{m}$ and period $\Lambda = 50\text{ nm}$. Inset figure shows heat flux as a function of temperature difference at 100 nm separation to highlight diode-like characteristics of different configurations.

far-field rectification being about the same. Rectification is stronger in near-field because of the asymmetry in heat flux due to different levels of tunneling of surface waves across the two interfaces. We now consider case III where thin film of VO_2 is replaced by a 1-D grating structure of height $h = 0.5\text{ }\mu\text{m}$, period $\Lambda = 50\text{ nm}$ and filling ratio $\phi = 0.3$. The passive side

remains the same as in case II. This configuration shows a significant enhancement in rectification and rectification value reaches around 14 at the gap of 100 nm. **Figure 7** also shows dependence of rectification ratio on gap for an alternative design (case IV) depicted in **Figure 6(b)**. This design has a 1-D triangular structure of height $h = 0.5 \mu\text{m}$ and period $\Lambda = 50 \text{ nm}$ on active side. While this structure shows a similar trend as case III, a sharp increase in rectification ratio can be seen at smaller gaps. Rectification ratio of 16 is reached at 100 nm gap. Although results for the distances smaller than 100 nm may not be accurate completely as gap becomes comparable to the grating period (displayed using dashed lines in **Figure 7**). The trend is noteworthy for the triangular structure (case IV) as rectification ratio keeps increasing to higher values for shorter distances. Numerical methods such as Wiener chaos expansion method [54] can be employed for calculation of near-field heat flux for distances shorter than the grating period. **Figure 7** inset displays heat flux versus temperature difference for the four cases studied. Difference between slopes for forward and reverse bias is obvious. Diode-like characteristics are apparent especially for designs based on rectangular and triangular gratings.

Different materials such as SiO_2 , SiC, BN, gold and polystyrene and structures (thin film or bulk) can be used on passive side and strongly influence rectification. When $1 \mu\text{m}$ layer of BN is used over reflecting gold surface on passive side, it results in maximum rectification for case II. The choice of passive structure used here may not remain optimal when active structure is modified. In order to emphasize the effect of 1-D gratings on active side, we have used the same structure on passive side for cases II, III and IV.

To illustrate why grating structure enhances the thermal rectification, we plot energy transmission coefficient $\xi(\omega, k_p)$ across the interfaces of thermal diode for case II (**Figure 8(a)** and **(b)**) and Case III (**Figure 8(c)** and **(d)**) at a gap of 100 nm. Here $k_p c / \omega$ is normalized parallel wavevector (for details on $\xi(\omega, k_p)$). For both cases, transmission coefficient is close to unity for forward bias well beyond light line ($k_p c / \omega = 1$). Transmission is high for two prominent frequencies that are close to characteristic wavelengths of BN (7.6 and $9.8 \mu\text{m}$), as shown by dashed lines. Since metallic VO_2 does not support surface phonon polariton in the infrared region [26], near-field radiative transfer is mainly attributed to the symmetric and antisymmetric surface phonons supported by the BN layer ($k_p c / \omega \gg 1$ in **Figure 8**). In addition, there exists a secondary contribution due to Fabry-Perot modes and frustrated modes ($k_p c / \omega \approx 1$) in the near-field regime. High energy transmission in forward bias is due to tunneling of surface waves across interfaces. In reverse bias, although both BN and insulator VO_2 support surface phonon modes, they do not overlap (see **Figure 9**) and near-field radiative transfer is dominated by non-resonant surface waves. In addition, surface phonons of insulator VO_2 occur in frequency range where BN has low extinction coefficient ($\kappa \approx 0$), and vice versa. As a result, tunneling between BN and insulator VO_2 is much weaker than that of BN and metallic VO_2 , that leads to thermal rectification. Observe that when thin film of VO_2 is replaced by a 1-D rectangular grating, transmission coefficient for reverse bias is reduced as seen in **Figure 8(b)** and **(d)**. Reduction in transmission coefficient comes from the presence of grating which suppresses the tunneling of surface waves supported by insulator VO_2 and BN. Tunneling between BN and metallic VO_2 however is relatively unchanged (**Figure 8(a)** and **(c)**). Consequently, a higher rectification is achieved. Resulting difference in spectral heat fluxes can also be observed.

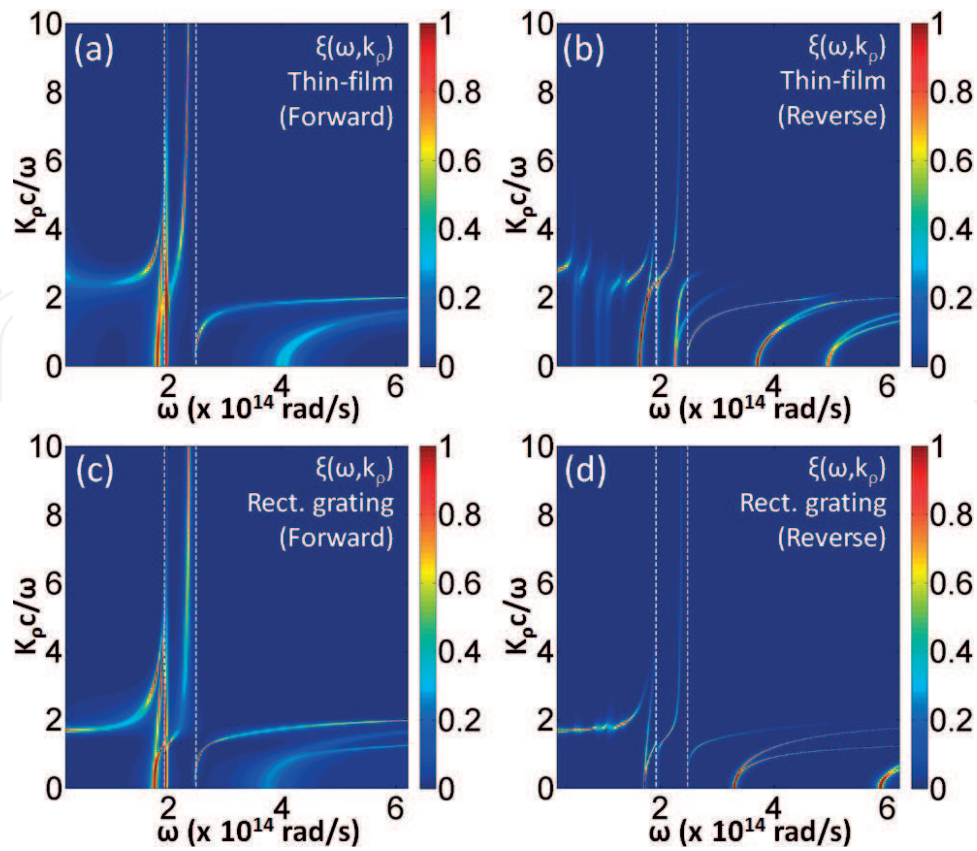


Figure 8. Coefficient of energy transmission $\xi(\omega, k_p)$ across the two interfaces of thermal diode plotted against angular frequency ω and normalized parallel wavevector $k_p c/\omega$ for (a) case II: Forward bias, (b) case II: Reverse bias, (c) case III: Forward bias, and (d) case III: Reverse bias.

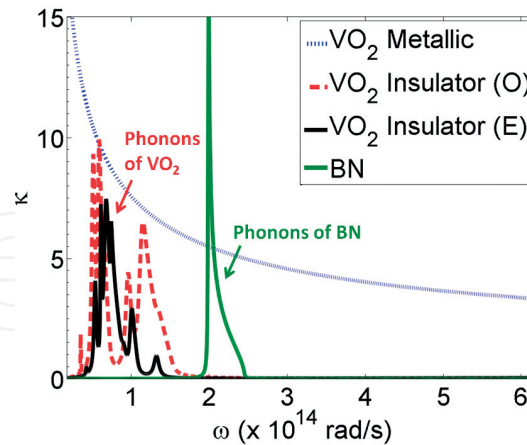


Figure 9. Extinction coefficient of metallic VO_2 , insulator VO_2 (ordinary and extraordinary modes) and BN.

Spectral heat flux $dq/d\lambda$ in forward and reverse bias for the cases II and III at gap of 100 nm is plotted in **Figure 10**. For the structure with thin film of VO_2 , majority of spectrum (solid lines) shows higher heat flux in forward direction than the reverse, which explains the rectification ratio being more than 1. The two prominent peaks that can be seen in the

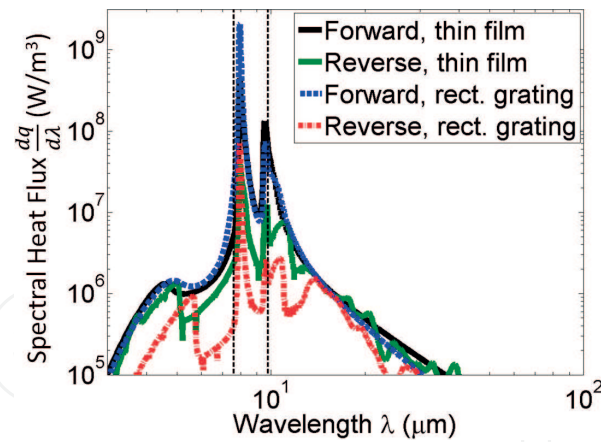


Figure 10. Comparison of spectral heat fluxes in forward and reverse bias for case II with a VO₂ thin film and case III with a rectangular grating structure. (Horizontal axis starts at 3 μm.)

spectrum are due to the frustrated modes of BN that happen around the characteristic wavelengths of BN at 7.6 and 9.8 μm. It is apparent that tunneling of surface waves across interfaces of insulator VO₂ and BN is weaker as the peaks have a reduced intensity. When the 1 μm thin film of VO₂ is replaced by the grating structure (dashed lines), forward heat flux shows little change. However, reverse heat flux is considerably reduced. It gives rise to an increased rectification.

One can analyze possible parameters that can influence the rectification for the design using 1-D rectangular grating (case III) for a gap of 100 nm in **Figure 11**. Filling ratio is fixed to 0.3 and the grating height is varied from 0.1 to 0.9 μm (dashed line). We observe that peak rectification ratio is achieved when grating height is around 0.5 μm. Solid line in **Figure 9** shows variation

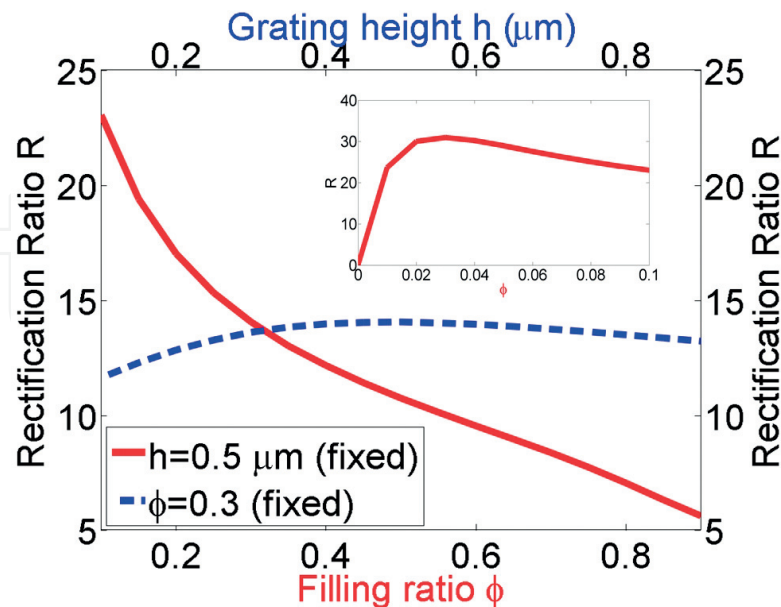


Figure 11. Effect of design parameters (filling ratio ϕ and grating height h) on the rectification ratio of thermal diode using rectangular gratings. Inset figure shows variation of rectification ratio near zero filling ratio. (Horizontal axis in main figure starts at 0.1).

in filling ratio for fixed grating height of 0.5 μm . Dependence of rectification on filling ratio is clearly stronger, as it directly affects the optical properties of grating structure therefore influencing the surface waves across the interfaces. For higher filling ratios, rectification values are lower, and understandably, are close to what is predicted for a thin film design (case II). Thermal rectification even higher than 20 can be predicted at smaller filling ratios. Rectification reaches maximum value when filling ratio is around 0.03, and it becomes zero when filling ratio is zero (**Figure 9** inset). However, filling ratio of 0.03 is impractical as grating period is 50 nm. Another parameter of interest would be grating period. Since our focus is on gap of 100 nm we have to limit ourselves to periods less than 100 nm. As the period is much smaller than the dominant thermal wavelength, it has virtually no effect on rectification.

4. Methods

To calculate heat flux for forward and reverse bias across near-field thermal diode, we can use the well-known expression of near-field radiative transfer obtained through dyadic Green's function formalism [55]. Radiative transfer between closely spaced objects can be calculated by

$$Q_{1 \rightarrow 2}(T_1, T_2, L) = \int_0^\infty \frac{d\omega}{2\pi} [\Theta(\omega, T_1) - \Theta(\omega, T_2)] T_{1 \rightarrow 2}(\omega, L) \quad (1)$$

where $\Theta(\omega, T) = (\hbar\omega/2)\coth(\hbar\omega/2k_B T)$ is the energy of harmonic oscillator at frequency ω and temperature T , \hbar is the reduced Planck constant, and k_B is the Boltzmann constant. The function $T_{1 \rightarrow 2}(\omega, L)$ is known as the spectral transmissivity in radiative transfer between media 1 and 2 separated of distance L [26, 32, 36, 55] and is expressed as

$$T_{1 \rightarrow 2}(\omega) = \int_0^\infty \frac{k_p dk_p}{2\pi} \xi(\omega, k_p) \quad (2)$$

Here, k_p is the parallel component of wavevector and the integrand is known as energy transmission coefficient and can be defined as

$$\xi(\omega, k_p \leq \omega/c) = \sum_{\mu=s, p} \frac{(1 - |\tilde{R}_1^{(\mu)}|^2)(1 - |\tilde{R}_2^{(\mu)}|^2)}{|1 - \tilde{R}_1^{(\mu)} \tilde{R}_2^{(\mu)} e^{2jk_z L}|^2} \quad (3a)$$

$$\xi(\omega, k_p > \omega/c) = \sum_{\mu=s, p} \frac{4\Im(\tilde{R}_1^{(\mu)})\Im(\tilde{R}_2^{(\mu)})e^{-2|k_z|L}}{|1 - \tilde{R}_1^{(\mu)} \tilde{R}_2^{(\mu)} e^{-2|k_z|L}|^2} \quad (3b)$$

where $\tilde{R}_1^{(\mu)}$ and $\tilde{R}_2^{(\mu)}$ are polarization dependent reflection coefficients of the two half spaces, $\mu = s$ (or p) refers to transverse electric (or magnetic) polarization, and k_z is the z -component of wavevector in vacuum. $k_p \leq \omega/c$ and $k_p > \omega/c$ correspond to propagating and evanescent

modes, respectively. For a structure having N -layer media having $(N - 1)$ interfaces, by solving the boundary conditions at the interfaces, one can obtain the expression for the generalized reflection coefficient at the interface between regions i and $i + 1$ [56],

$$\tilde{R}_{i,i+1}^{(\mu)} = \frac{R_{i,i+1}^{(\mu)} + \tilde{R}_{i+1,i+2}^{(\mu)} e^{2jk_{i+1,z}(d_{i+1}-d_i)}}{1 + R_{i,i+1}^{(\mu)} \tilde{R}_{i+1,i+2}^{(\mu)} e^{2jk_{i+1,z}(d_{i+1}-d_i)}} \quad (4)$$

where $R_{i,i+1}^{(\mu)}$ is the Fresnel reflection coefficient at the interface between the layers i and $i + 1$, and $\tilde{R}_{i+1,i+2}^{(\mu)}$ is the generalized reflection coefficient at the interface between the layers $i + 1$ and $i + 2$, $z = -d_i$ is the location of the i th interface. $k_{i,z} = \sqrt{\epsilon_i(\omega)\omega^2/c^2 - k_p^2}$ is the normal z -component of the wave vector in medium i , wherein $\epsilon_i(\omega)$ is the relative permittivity of the medium i as a function of angular frequency ω , c is the speed of light in vacuum. With $\tilde{R}_{N,N+1}^{(\mu)} = 0$, the above equation provides a recursive relation to calculate the reflection coefficients $\tilde{R}_{i,i+1}^{(\mu)}$ in all regions. For the far-field configuration, $\xi(\omega, k_p > \omega/c)$ is ignored as separation between the two half spaces is much larger than the thermal wavelength ($L \gg \lambda_{th}$). The hemispherical emissivity of the active component can be expressed as [32]

$$e(\omega) = \frac{c^2}{\omega^2} \int_0^{\omega/c} dk_p k_p \sum_{\mu=s,p} \left(1 - |\tilde{R}_h^{(\mu)}|^2 \right) \quad (5)$$

Note that the term for transmissivity has been omitted as a layer of gold makes the structure opaque.

Since the proposed designs involve 1-D grating structure of VO_2 in vacuum, we can use second order approximation of effective medium theory to obtain the dielectric properties given by the expressions [47, 27, 8]

$$\epsilon_{TE,2} = \epsilon_{TE,0} \left[1 + \frac{\pi^2}{3} \left(\frac{\Lambda}{\lambda} \right)^2 \phi^2 (1 - \phi)^2 \frac{(\epsilon_A - \epsilon_B)^2}{\epsilon_{TE,0}} \right] \quad (6a)$$

$$\epsilon_{TM,2} = \epsilon_{TM,0} \left[1 + \frac{\pi^2}{3} \left(\frac{\Lambda}{\lambda} \right)^2 \phi^2 (1 - \phi)^2 (\epsilon_A - \epsilon_B)^2 \epsilon_{TE,0} \left(\frac{\epsilon_{TM,0}}{\epsilon_A \epsilon_B} \right)^2 \right] \quad (6b)$$

where ϵ_A and ϵ_B are dielectric functions of the two materials (VO_2 and vacuum) in surface gratings, λ is the wavelength, Λ is grating period and filling ratio $\phi = w/\Lambda$ where w is width of VO_2 segment. The expressions for zeroth order effective dielectric functions $\epsilon_{TE,0}$ and $\epsilon_{TM,0}$ are given by [57, 58]

$$\epsilon_{TE,0} = \phi \epsilon_A + (1 - \phi) \epsilon_B \quad (7a)$$

$$\epsilon_{TM,0} = \left(\frac{\phi}{\epsilon_A} + \frac{1-\phi}{\epsilon_B} \right)^{-1} \quad (7b)$$

For triangular gratings as shown in **Figure 6(b)**, gratings can be treated as a composition of multiple layers of rectangular gratings each having decreasing filling ratio and period equal to that of parent grating [58]. It was observed that slicing the triangular structure into 100 layers is sufficient to achieve converging values of near-field heat flux.

Effective medium approximation (EMA) holds true when grating period is much less than wavelength of interest [59]. As this study deals with temperatures around 341 K, grating period (50 nm) is much less than the thermal wavelength ($\sim 8.5 \mu\text{m}$). Thus the condition of EMA is satisfied. When dealing with near-field radiative transfer pertaining to periodic gratings, criterion for the validity of EMA is somewhat different and effective medium theory holds true as long as gap between the planar structures (100 nm in this case) is greater than the grating period [60] (see discussions about dashed lines in **Figure 7**).

VO_2 in insulator state (below 341 K) is anisotropic. In a plane perpendicular to optical axis ($x - y$ plane in our case) known as ordinary mode, its dielectric function is ϵ_O and it is ϵ_E along the optical axis (z axis, extraordinary mode). Both ϵ_O and ϵ_E can be calculated using classical oscillator formula $\epsilon(\omega) = \epsilon_\infty + \sum_{i=1}^N \frac{S_i \omega_i^2}{\omega_i^2 - j\gamma_i \omega - \omega^2}$. Experimental values of high-frequency constant ϵ_∞ , phonon frequency ω_i , scattering rate γ_i and oscillator strength S_i can be found in Ref. [61]. Here, j is the imaginary unit. There exist eight phonon modes for ordinary and nine phonon modes for extraordinary dielectric function. In metallic state, VO_2 is isotropic and Drude model [61] is used to describe the dielectric function that is given by $\epsilon(\omega) = \frac{-\omega_p^2 \epsilon_\infty}{\omega^2 - j\omega\Gamma}$.

Dielectric function for BN [62] is of the form $\epsilon(\omega) = \epsilon_\infty \frac{(\omega^2 - \omega_{LO}^2 + j\omega\gamma)}{(\omega^2 - \omega_{TO}^2 + j\omega\gamma)}$. Here ω_{TO} and ω_{LO} are transverse and longitudinal optical phonon frequencies and γ is the damping constant. The values of ϵ_∞ , ω_{TO} , ω_{LO} and γ for BN are 4.46, 0.1309, 0.1616 and 6.55×10^{-4} eV respectively. Dielectric properties of gold can be found in Ref. [63].

5. Conclusion

We saw two configurations of radiative thermal diode that exploit metal-insulator transition of VO_2 . The VO_2 based far-field radiative thermal diode structure presented here has a high rectification ratio of 11.3. The active component of the device has a tri-layer structure consisting thin films of VO_2 , KBr and gold. As VO_2 undergoes phase change around 341 K, reflecting properties of the surface are dramatically changed in the spectral region that contributes to significant amount of thermal radiation. Facilitated by Fabry-Perot type of resonance around $5.3 \mu\text{m}$, metallic VO_2 makes the structure behave like a wide-angle antireflection coating while insulating VO_2 makes it highly reflecting. As a result, high degree of asymmetry in radiative heat transfer is predicted across the tri-layer structure and a blackbody. Contrasting reflecting properties of the structure can be explained using constructive and destructive interference of partial reflections across the interfaces. Layer thicknesses are optimized to maximize rectification. Thermal rectification greater than 11 is predicted for temperature difference of 20 K and it is highest among far-field radiative diodes that have been

studied. Possibility of attaining higher rectification could be investigated in future by using alternate transparent materials, thinner films of VO₂ and/or using more number of alternating VO₂/dielectric layers. Such devices can find numerous applications such as thermal logic devices and thermal management systems. In the near-field configuration, it has been demonstrated that an enhanced thermal rectification can be achieved using 1-D grating of phase change material VO₂. The calculations presented here indicate that a very high value of rectification ratio (~ 16) can be obtained at a gap of 100 nm. Rectification ratio can be optimized by tuning parameters such as grating height and especially, filling ratio. Materials and structures on passive side also play a significant role in the rectification. Improved rectification is attributed to reduced tunneling of surface waves across the interfaces for reverse bias. Rectification ratio can be further increased to much higher values for distance shorter than 100 nm and it is a viable candidate for future investigations.

Acknowledgements

This project was supported in part by a National Science Foundation through grant number 1655221, Institutional Development Award (IDeA) Network for Biomedical Research Excellence from the National Institute of General Medical Sciences of the National Institutes of Health under grant number P20GM103430, and Rhode Island Foundation Research Grant number 20164342.

Conflict of interest

The authors declare no competing interests.

Author details

Alok Ghanekar, Yanpei Tian and Yi Zheng*

*Address all correspondence to: zheng@uri.edu

Department of Mechanical, Industrial and Systems Engineering, University of Rhode Island, Kingston, RI, USA

References

- [1] Li B, Wang L, Casati G. Thermal diode: Rectification of heat flux. *Physical Review Letters*. 2004;**93**(18):184301
- [2] Li B, Wang L, Casati G. Negative differential thermal resistance and thermal transistor. *Applied Physics Letters*. 2006;**88**(14):143501

- [3] Wang L, Li B. Thermal memory: A storage of phononic information. *Physical Review Letters*. 2008;**101**(26):267203
- [4] Kobayashi W, Teraoka Y, Terasaki I. An oxide thermal rectifier. *Applied Physics Letters*. 2009;**95**(17):171905
- [5] Sawaki D, Kobayashi W, Moritomo Y, Terasaki I. Thermal rectification in bulk materials with asymmetric shape. *Applied Physics Letters*. 2011;**1102**:4182
- [6] Kobayashi W, Sawaki D, Omura T, Katsufuji T, Moritomo Y, Terasaki I. Thermal rectification in the vicinity of a structural phase transition. *Applied Physics Express*. 2012;**5**(2):027302
- [7] Chang CW, Okawa D, Majumdar A, Zettl A. Solid-state thermal rectifier. *Science*. 2006;**314**(5802):1121-1124
- [8] Martínez-Pérez MJ, Fornieri A, Giazotto F. Rectification of electronic heat current by a hybrid thermal diode. *Nature Nanotechnology*. 2015;**10**(4):303-307
- [9] Ben-Abdallah P, Biehs S-A. Near-field thermal transistor. *Physical Review Letters*. 2014;**112**(4):044301
- [10] Ben-Abdallah P, Biehs S-A. Phase-change radiative thermal diode. *Applied Physics Letters*. 2013;**103**(19):191907
- [11] Otey CR, Lau WT, Fan S. Thermal rectification through vacuum. *Physical Review Letters*. 2010;**104**(15):154301
- [12] Chen Z, Wong C, Lubner S, Yee S, Miller J, Jang W, Hardin C, Fong A, Garay JE, Dames C. A photon thermal diode. *Nature Communications*. 2014;**5**
- [13] Wang L, Li B. Phononics gets hot. *Physics World*. 2008;**21**:27-29
- [14] Wang L, Li B. Thermal logic gates: Computation with phonons. *Physical Review Letters*. 2007;**99**(17):177208
- [15] Ben-Abdallah P, Biehs S-A. Towards boolean operations with thermal photons. *Physical Review B*. 2016;**94**(24):241401
- [16] Li N, Ren J, Wang L, Zhang G, Hänggi P, Li B. Colloquium: Phononics: Manipulating heat flow with electronic analogs and beyond. *Reviews of Modern Physics*. 2012;**84**(3):1045
- [17] Song B, Fiorino A, Meyhofer E, Reddy P. Near-field radiative thermal transport: From theory to experiment. *AIP Advances*. 2015;**5**(5):053503
- [18] Yang Y, Basu S, Wang L. Radiation-based near-field thermal rectification with phase transition materials. *Applied Physics Letters*. 2013;**103**(16):163101
- [19] Huang J, Li Q, Zheng Z, Xuan Y. Thermal rectification based on thermochromic materials. *International Journal of Heat and Mass Transfer*. 2013;**67**:575-580
- [20] Nefzaoui E, Joulain K, Drevillon J, Ezzahri Y. Radiative thermal rectification using superconducting materials. *Applied Physics Letters*. 2014;**104**(10):103905

- [21] Joulain K, Ezzahri Y, Drevillon J, Ben-Abdallah P. Modulation and amplification of radiative far field heat transfer: Towards a simple radiative thermal transistor. *Applied Physics Letters*. 2015;**106**(13):133505
- [22] Van Zwol PJ, Joulain K, Abdallah PB, Greffet JJ, Chevrier J. Fast nanoscale heat-flux modulation with phase-change materials. *Physical Review B*. 2011;**83**(20):201404
- [23] Van Zwol PJ, Ranno L, Chevrier J. Tuning near field radiative heat flux through surface excitations with a metal insulator transition. *Physical Review Letters*. 2012;**108**(23):234301
- [24] Menges F, Dittberner M, Novotny L, Donata P, Parkin SSP, Spieser M, Riel H, Gotsmann B. Thermal radiative near field transport between vanadium dioxide and silicon oxide across the metal insulator transition. *Applied Physics Letters*. 2016;**108**(17):171904
- [25] Ghanekar A, Ji J, Zheng Y. High-rectification near-field thermal diode using phase change periodic nanostructure. *Applied Physics Letters*. 2016;**109**(12):123106
- [26] Yang Y, Basu S, Wang L. Vacuum thermal switch made of phase transition materials considering thin film and substrate effects. *Journal of Quantitative Spectroscopy and Radiative Transfer*. 2015;**158**:69-77
- [27] Prod'homme H, Ordonez-Miranda J, Ezzahri Y, Drevillon J, Joulain K. Optimized thermal amplification in a radiative transistor. *Journal of Applied Physics*. 2016;**119**(19):194502
- [28] Zhu L, Otey CR, Fan S. Negative differential thermal conductance through vacuum. *Applied Physics Letters*. 2012;**100**(4):044104
- [29] Lee K-T, Ji C, Jay Guo L. Wide-angle, polarization-independent ultrathin broadband visible absorbers. *Applied Physics Letters*. 2016;**108**(3):031107
- [30] Zheng Y, Ghanekar A. Radiative energy and momentum transfer for various spherical shapes: A single sphere, a bubble, a spherical shell, and a coated sphere. *Journal of Applied Physics*. 2015;**117**(6):064314
- [31] Zhu L, Otey CR, Fan S. Ultrahigh-contrast and large-bandwidth thermal rectification in near-field electromagnetic thermal transfer between nanoparticles. *Physical Review B*. 2013;**88**(18):184301
- [32] Ghanekar A, Lin L, Junwei S, Sun H, Zheng Y. Role of nanoparticles in wavelength selectivity of multilayered structures in the far-field and near-field regimes. *Optics Express*. 2015;**23**(19):A1129-A1139
- [33] Ghanekar A, Lin L, Zheng Y. Novel and efficient mie-metamaterial thermal emitter for thermophotovoltaic systems. *Optics Express*. 2016;**24**(10):A868-A877
- [34] Rinnerbauer V, Lenert A, Bierman DM, Yeng YX, Chan WR, Geil RD, Senkevich JJ, Joannopoulos JD, Wang EN, Soljačić M, et al. Metallic photonic crystal absorber-emitter for efficient spectral control in high- temperature solar thermophotovoltaics. *Advanced Energy Materials*. 2014;**4**(12)

- [35] Chou JB, Yeng YX, Lenert A, Rinnerbauer V, Celanovic I, Soljačić M, Wang EN, Kim S-G. Design of wide-angle selective absorbers/emitters with dielectric filled metallic photonic crystals for energy applications. *Optics Express*. 2014;**22**(101):A144-A154
- [36] Biehs S-A, Rosa FSS, Ben-Abdallah P. Modulation of near-field heat transfer between two gratings. *Applied Physics Letters*. 2011;**98**(24):243102
- [37] Zheludev NI, Kivshar YS. From metamaterials to metadevices. *Nature Materials*. 2012;**11**(11):917-924
- [38] Nanfang Y, Capasso F. Flat optics with designer metasurfaces. *Nature Materials*. 2014;**13**(2):139-150
- [39] Selim Ünlü M, Strite S. Resonant cavity enhanced photonic devices. *Journal of Applied Physics*. 1995;**78**(2):607-639
- [40] Kishino K, Unlu MS, Chyi JJ, Reed J, Arsenault L, Morkoc H. Resonant cavity-enhanced (rce) photodetectors. *IEEE Journal of Quantum Electronics*. 1991;**27**(8):2025-2034
- [41] Fante RL, McCormack MT. Reflection properties of the salisbury screen. *IEEE Transactions on Antennas and Propagation*. 1988;**36**(10):1443-1454
- [42] Raaijmakers J, Simovski CR, Tretyakov SA. Thin perfect absorbers for electromagnetic waves: Theory, design, and realizations. *Physical Review Applied*. 2015;**3**(3):037001
- [43] Bosman H, Lau YY, Gilgenbach RM. Microwave absorption on a thin film. *Applied Physics Letters*. 2003;**82**(9):1353-1355
- [44] Hägglund C, Peter Apell S, Kasemo B. Maximized optical absorption in ultrathin films and its application to plasmon-based two-dimensional photovoltaics. *Nano Letters*. 2010;**10**(8):3135-3141
- [45] Mingbo P, Feng Q, Wang M, Hu C, Huang C, Ma X, Zhao Z, Wang C, Luo X. Ultrathin broadband nearly perfect absorber with symmetrical coherent illumination. *Optics Express*. 2012;**20**(3):2246-2254
- [46] Nefzaoui E, Drevillon J, Ezzahri Y, Joulain K. Simple far-field radiative thermal rectifier using fabry-perot cavities based infrared selective emitters. *Applied Optics*. 2014;**53**(16):3479-3485
- [47] Kats MA, Sharma D, Lin J, Genevet P, Blanchard R, Yang Z, Mumtaz Qazilbash M, Basov DN, Ramanathan S, Capasso F. Ultra-thin perfect absorber employing a tunable phase change material. *Applied Physics Letters*. 2012;**101**(22):221101
- [48] Taylor S, Yang Y, Wang L. Vanadium dioxide based fabry-perot emitter for dynamic radiative cooling applications. *Journal of Quantitative Spectroscopy and Radiative Transfer*; 2017
- [49] Qazilbash MM, Brehm M, Andreev GO, Frenzel A, Ho P-C, Chae B-G, Kim B-J, Yun SJ, Kim H-T, Balatsky AV, Shpyrko OG. Infrared spectroscopy and nano-imaging of the insulator-to-metal transition in vanadium dioxide. *Physical Review B*. 2009;**79**(7):075107

- [50] Frenzel A, Qazilbash MM, Brehm M, Chae B-G, Kim B-J, Kim H-T, Balatsky AV, Keilmann F, Basov DN. Inhomogeneous electronic state near the insulator-to-metal transition in the correlated oxide VO_2 . *Physical Review B*. 2009;**80**(11):115115
- [51] Ordonez-Miranda J, Ezzahri Y, Drevillon J, Joulain K. Transistorlike device for heating and cooling based on the thermal hysteresis of VO_2 . *Physical Review Applied*. 2016;**6**(5):054003
- [52] Kats MA, Capasso F. Optical absorbers based on strong interference in ultra-thin films (laser photonics rev. 10 (5)/2016). *Laser & Photonics Reviews*. 2016;**10**(5):699-699
- [53] Narayanaswamy A, Mayo J, Canetta C. Infrared selective emitters with thin films of polar materials. *Applied Physics Letters*. 2014;**104**(18):183107
- [54] Liu B, Shen S. Broadband near-field radiative thermal emitter/absorber based on hyperbolic metamaterials: Direct numerical simulation by the wiener chaos expansion method. *Physical Review B*. 2013;**87**(11):115403
- [55] Narayanaswamy A, Zheng Y. A Green's function formalism of energy and momentum transfer in fluctuational electrodynamics. *Journal of Quantitative Spectroscopy and Radiative Transfer*. 2014;**132**:12-21
- [56] Chew WC. *Waves and Fields in Inhomogeneous Media*. New York, NY: IEEE Press; 1995
- [57] Raguin DH, Michael Morris G. Antireflection structured surfaces for the infrared spectral region. *Applied Optics*. 1993;**32**(7):1154-1167
- [58] Glytsis EN, Gaylord TK. High-spatial-frequency binary and multilevel stairstep gratings: Polarization-selective mirrors and broadband antireflection surfaces. *Applied Optics*. 1992;**31**(22):4459-4470
- [59] Chen Y-B, Zhang ZM, Timans PJ. Radiative properties of patterned wafers with nanoscale linewidth. *Journal of Heat Transfer*. 2007;**129**(1):79-90
- [60] Liu XL, Bright TJ, Zhang ZM. Application conditions of effective medium theory in near-field radiative heat transfer between multilayered metamaterials. *Journal of Heat Transfer*. 2014;**136**(9):092703
- [61] Barker AS Jr, Verleur HW, Guggenheim HJ. Infrared optical properties of vanadium dioxide above and below the transition temperature. *Physical Review Letters*. 1966;**17**(26):1286
- [62] Palik ED. *Handbook of Optical Constants of Solids*. Vol. 3. Cambridge, Massachusetts: Academic Press; 1998
- [63] Johnson PB, Christy R-W. Optical constants of the noble metals. *Physical Review B*. 1972;**6**(12):4370

